Diaminomaleonitrile-functionalised Schiff Bases: Synthesis, Solvatochromism, and Lysosome-specific Imaging

Siyang Ding,[A] Bicheng Yao,[A] Moore Zhe Chen,[B] Chuanxin Liu,[C] Tze Cin Owyong,[A] Angus Johnston[B] and Yuning Hong[A,D]

[A]Department of Chemistry and Physics, La Trobe Institute for Molecular Science, La Trobe University, Melbourne, Vic. 3086, Australia.

[B]ARC Centre of Excellence in Convergent Bio-Nano Science and Technology and Drug Delivery, Disposition and Dynamics, Monash Institute of Pharmaceutical Sciences, Monash University, 381 Royal Parade, Parkville, Vic. 3052, Australia.

[C]Department of Biochemistry and Genetics, La Trobe Institute for Molecular Science, La Trobe University, Melbourne, Vic. 3086, Australia.

[D]Corresponding author. Email: y.hong@latrobe.edu.au

ABSTRACT: Design of novel organic fluorescent molecules with aggregation-induced emission (AIE) properties has been a research focus in the past two decades. In this work, we reported the photophysical studies and potential applications of a series of AIE-active luminogens based on a small building block, diaminomaleonitrile Schiff base. By taking advantages of easy-approachable synthetic procedures and excellent optical properties of this system, we further explored the applications of this system for cell imaging.

Introduction

Typical conventional fluorophores, such as fluorescein, boron dipyrromethene (BODIPY), coumarin, etc., suffer from a common problem of aggregation-caused quenching (ACQ), which often hampers their applications especially in biological systems. On the other hand, aggregation-induced emission-active fluorogens (AIEgens) are emissive upon aggregating but nearly non-emissive in the solution, which was firstly demonstrated by Tang et al in 2001[1]. The main mechanism of AIE phenomenon was proposed to the restriction of intramolecular rotation (RIR)[2-5] and restriction of intramolecular vibrations (RIV)[6], or in general, restriction of intramolecular motions (RIM)[7-8]. Currently, numerous fluorophore cores with AIE properties have been reported and many research efforts have been oriented to the exploration of their distinct structure-property relationships. Examples of classic AIE systems include silole[9-11], tetraphenylethene (TPE)[12-13] and so on. Among them, bulky silole-cored compounds are often cell impermeable, while TPE analogues normally can only be excited at the wavelength below 400 nm, which is not optimal for most confocal microscopes with 405 nm laser as the shortest wavelength for excitation. Extending the conjugation system of TPE can effectively shift the excitation above 400 nm but usually requires complicating synthesis and purification steps. Therefore, it is still in high demand to discover small building blocks for constructing red-shifted biocompatible AIEgens. By incorporating the electron donor (D) and acceptor (A) pairs to form a large bathochromic shift in emission colour, Han et al firstly reported a diaminomaleonitrile-based AIE molecule with the D-π-A structure[14]. Since then this diaminomaleonitrile-functionalised system has been well developed by switching donor groups[15] or adding additional functional groups[16]. Their photophysical properties in both crystalline and amorphous states, as well as their application for enzymatic activity has been reported[16].

Lysosomes, long known as cellular terminal degradation stations, are a type of subcellular organelle that has been found to be responsible for the digestion of denatured proteins and dysfunctional organelles[17]. The acidic environments in lysosomes (pH 4.5-5.5) can facilitate numerous cellular degradation pathways, including autophagy[18]. Thus, visualizing and tracking lysosomes will enrich the insight into certain metabolism activities. However, recent studies suggested that some of commercially available lysosomal trackers came across severe drawbacks, such as weak photostability or intolerance of cell fixation procedure. Therefore, it is imperative to develop a proper lysosome-targeting probe which can meet the growing demand of easy-handling flexible applicability.

In this work, three new diaminomaleonitrile-based molecules were designed and successfully synthesized. As a supplement of this system, we combined two of previously published molecules into the overall discussion, aiming to provide a comprehensive structural-property relationship of diaminomaleonitrile-functionalized Schiff bases. In addition, by introducing the alkylated morpholine into structure design, the resulting fluorogen can specifically target and image lysosomes in the cells.

Results and Discussion

A series of diaminomaleonitrile-functionalized Schiff bases (**Scheme 1**) were synthesized according to the previously reported method[14] (**Scheme S1** in Supplementary Materials). The intermediate product **3** was prepared by the two-step modification, involving with Williamson ether synthesis and conjugation with the morpholine group. The morpholine

group with moderate alkalinity is employed for pH sensing[19] as well as for improving the solubility of Lyso-BAM, making it more suitable for biological applications. The subsequent additions of amines to aldehydes were conducted under mildly acidify conditions, affording a good yield of more than 60%. All products were fully characterized by ^{1}H and ^{13}C NMR and high-resolution mass spectrometry (HRMS), which gave satisfactory analysis results corresponding to their chemical structures (Supplementary Materials). In addition, Et-BAM and Lyso-BAM are soluble in common organic solvents such as chloroform, THF, acetone, ethyl acetate (EA) and dimethyl sulfoxide (DMSO), whereas the other three molecules can only be dissolved in DMSO and show poor solubility in most of other organic solvents.

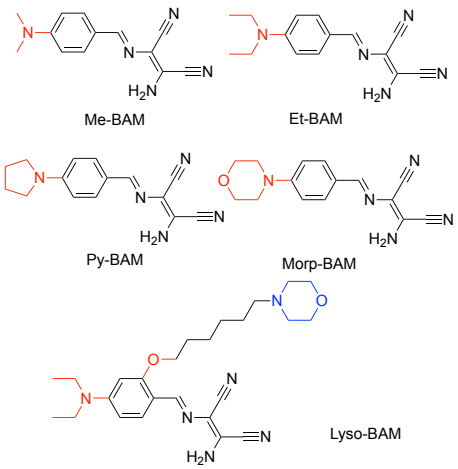

Scheme 1. Chemical structures of diaminomaleonitrile Schiff bases.

The photophysical properties of these five compounds were carefully characterised in order to investigate their applications. As shown in **Figure 1A**, Py-BAM and Et-BAM exhibited very similar absorption bands peaked at 438 nm in DMSO, while the absorption spectra of Me-BAM and Morp-BAM showed blue-shift of 429 and 409 nm, respectively, which may result from less electron donating abilities of the dimethylamine and morpholine groups. On the contrary, owing to the contribution of the additional alkyl ether group to conjugation, the absorption maximum of Lyso-BAM processed a small red-shift from 438 nm (Et-BAM) to 444 nm. Their emission spectra were measured after exciting at their recorded absorption maxima (**Figure 1B** and **Table 1**). Results showed that all five compounds exhibited weak emission with maxima at around 508-520 nm in DMSO solution.

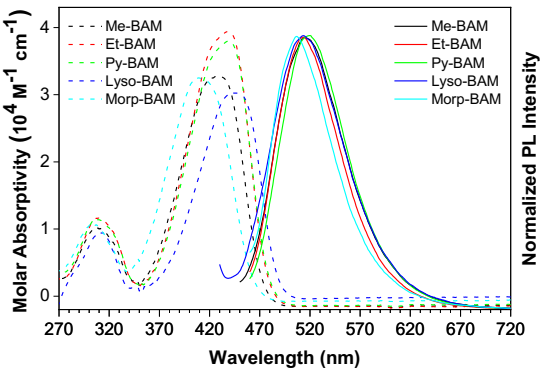

Figure 1. Molar absorptivity (dash line) and normalised emission spectra (solid line) in DMSO of BAMs. Concentration = 10 μM. Excitation wavelength: 430 (Me-BAM), 440 (Et-BAM), 440 (Py-BAM), 410 (Morp-BAM) and 440 nm (Lyso-BAM).

The photophysical properties of BAMs in solvents with different polarity were analysed, shown in **Figure 2** and **Figure S1**. The absorption maxima of the five compounds were obtained from the UV-vis spectra and the corresponding wavelengths of absorption maxima were used as excitation wavelength for recording the photoluminescence (PL). The Stokes shifts of all compounds as a function of solvent polarity were graphed in the Lippert[20]-Mataga[21] solvatochromism plot (**Figure 2**).

Table 1 Photophysical properties of BAMs.

Compounds	Absorbance λ_{max}[a] (nm)	Molar Absorptivity at λ_{max} (M^{-1} cm^{-1})	PL in Solution λ_{max}[a] (nm)
Me-BAM	429	3.27×10^4	518
Et-BAM	438	3.94×10^4	516
Py-BAM	438	3.80×10^4	521
Morp-BAM	409	3.25×10^4	513
Lyso-BAM	444	3.02×10^4	508

[a]Measured in DMSO solutions.

Me-BAM exhibited a small shift in the absorption maxima ranging from 409 to 436 nm in different solvents (**Figure S1A**). It was notable that the absorption spectrum of Me-BAM in water was remarkedly weaker and broader than those in other solvents, which may result from its poor solubility and aggregate formation in water. Interestingly, dichloromethane (DCM) caused a red shift and a pronounced shoulder at the longer wavelength (500 nm). The emission maxima of Me-BAM in different solvents were recorded to range from 434 to 518 nm (**Figure 2A**); as a distinct exception, water induced a significant red-shift to 601 nm. Stokes shifts of Me-BAM were mostly proportional to solvent polarities, suggesting it possesses positive solvatochromism like most of the fluorophores with push-pull structural feature (**Figure 2B**).

The absorption maxima of Et-BAM ranged from 363-438 nm in different solvents, shown in **Figure S1B**. In contrast to Me-BAM, the spectrum of Et-BAM in DCM showed a conspicuous blue shift, while the shoulder remained around the approximately same range (about 450-520 nm). Its emission maxima ranged from 484-519 nm (**Figure 2C**), where DCM caused a marked red shift compared to other solvents. Stokes shifts of Et-BAM had a moderate increase in more polar solvents (**Figure 2D**), which could be ascribed to the twisted intramolecular charge transfer (TICT) mechanism[14].

The absorption maxima of Py-BAM ranged from 369-498 nm, where the absorption spectrum in water exhibited a blue shift than those in other solvents (**Figure S1C**). Similar to the case of Me-BAM, DCM induced a small red-shift to 498 nm and a shoulder at longer wavelengths. As shown in **Figure 2C**, the emission maxima of Py-BAM ranged from 481-525 nm, whereas water caused a distinct red shift with spectrum peaked at 614 nm (**Figure 2F**). Stokes shifts of Py-BAM remained almost unchanged in different solvents (60-100 nm) except in water with the largest Stokes shift of 250 nm.

Morp-BAM showed nearly invariable absorption maxima ranged from 397-409 nm (**Figure S1D**), while its emission

maxima process proportional red-shift along with the increase of solvent polarities, showing typical positive solvatochromism (**Figure 2G and H**). The absorption maxima of Lyso-BAM ranged from 425-490 nm in different solvents. Similarly, DCM caused the most notable red shift. Unlike Morp-BAM, its emission maxima were around 500 nm except for a slight red shift to 525 nm in water. It can be observed that, apart from DCM and water, Stokes shifts of Lyso-BAM barely fluctuated in different solvents, indicating its stable and consistent PL properties.

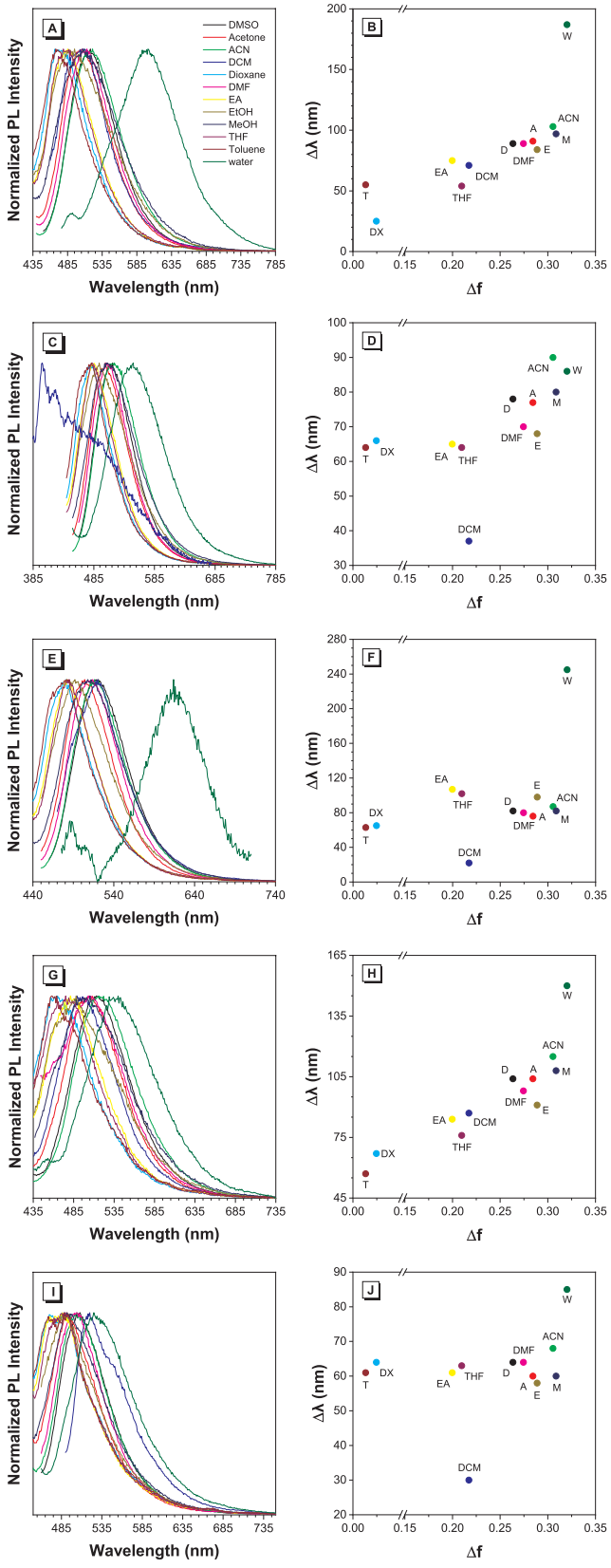

Figure 2. Normalized emission spectra and Lippert-Mataga solvatochromism plot of Me-BAM (A, B), Et-BAM (C, D), Py-BAM (E, F), Morp-BAM (G, H) and Lyso-BAM (I, J) in different solvents. Concentration = 10 μM. A = acetone, ACN = acetonitrile, D = DMSO, DX = 1,4-dioxane, E = ethanol, EA = ethyl acetate, M = methanol, T = toluene, W= water. Excitation wavelength listed in **Table S1**.

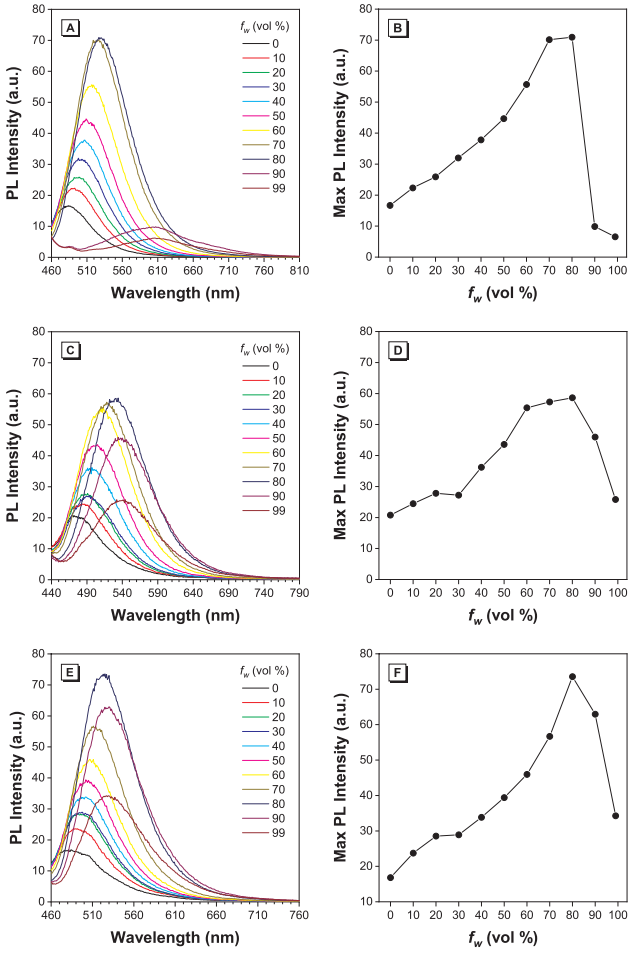

Figure 3. Emission intensity profiles of Py-BAM (A, B), Morp-BAM (C, D) and Lyso-BAM (E, F) in THF/water mixtures with different water fractions. Concentration = 10 μM. f_w and vol%: water volume fraction. Excitation wavelength: 440 (Py-BAM), 410 (Morp-BAM) and 440 nm (Lyso-BAM).

The AIE properties of all compounds were investigated in a series of THF/water mixtures with different volume fraction (**Figure 3**). Note that the AIE properties of Me-BAM[15] and Et-BAM[14] have previously been reported using the same solvent system, so here only data of the three novel compounds were shown. In general, the diluted THF solutions of Py-BAM, Morp-BAM and Lyso-BAM exhibited weak emission when photoexcited at 440, 420, and 440 nm, respectively. The PL intensity was gradually enhanced when the water fraction increased, companying with the striking emission maxima red shifting. In the THF-water mixture with 80 vol% of water, the fluorescence intensity of all three compounds reached highest point,

showing the classic AIE phenomenon. Further increasing the water fraction to 90 and 99%, however, led to the decrease of the fluorescence emission. Such changes could be attributed to two possibilities: the poor solubility/dispersibility of the dye molecules in water or the transition of crystalline to amorphous aggregates of the dyes, one of which might be more emissive than the other[14].

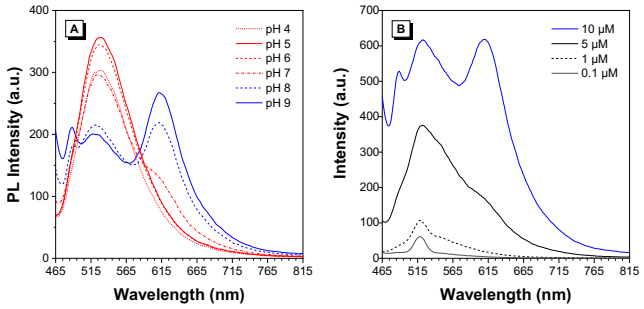

Figure 4. Emission spectra of Lyso-BAM (A) in buffers, pH values ranged from 4-9, concentration = 10 μM; (B) diluting in the pH 9 buffer with concentration ranged from 0.1 μM to 10 μM. λ_{ex} = 440 nm.

With pK_a at around 7, the nitrogen on the morpholine moiety of Lyso-BAM can be protonated at acidic condition. To investigate whether this process could affect the photophysical properties of the dye especially in biological systems, we measured the fluorescence spectrum of Lyso-BAM in different pH in the physiological range from 4 to 9. As shown in **Figure 4A**, in neutral pH 7, the emission maximum of Lyso-BAM was peaked at 528 nm with a shoulder peak at around 614 nm. The peak position at the shorter wavelength remained the same when the pH was lowered from from 7 to 4 with slight intensity increase at pH 5 and 6. The shoulder peak was not observed in acidic conditions. On the other hand, in basic condition, the intensity at 528 nm was decreased, while the original shoulder peak at 614 nm became predominant. In acidic condition where the morpholine unit is protonated, the positive charge could improve the solubility of the dye in water. Whereas in basic conditions, Lyso-BAM remains deprotonated, which facilitates the close packing of dye molecules in aqueous solution and thus intermolecular interactions that lead to a lower energy gap. The above hypothesis was examined by further diluting the Lyso-BAM into the pH 9 buffer. Results in **Figure 4B** showed that the peak around 614 nm gradually disappear with lower concentration of Lyso-BAM, indicating that the red-shifted peak was indeed induced by aggregates formed in the basic environment.

Before employing the Lyso-BAM to cell imaging, we firstly conducted AlamarBlue™ cell viability assay to evaluate its cytotoxicity. The viability of A549 cells after 40 min treatment of Lyso-BAM remained higher than 95%, with concentration up to 50 μM (**Figure S2**). The excellent biocompatibility and low cytotoxicity of Lyso-BAM prompted us to further investigate its applications in cell imaging.

In terms of sample preparation, we stained live A549 cells with Lyso-BAM-containing medium in the concentration of 25 μM. We further fixed the cells for the ease of sample handling for confocal microscopy imaging. It was found that Lyso-BAM processed extremely good cell permeability, entering cells within 40 min. In order to identify where the dye located in cells, we firstly used LysoTracker Deep Red™. However, we found the signals of LysoTracker disappeared when the cells were fixed[22]. We then used the A549-Lysosome20-mApple cell line stably expressing the mApple-fused lysosomal-associated membrane protein 1 (LAMP1)[23] to confirm the dye staining localization. **Figure 5** and **6** indicated that most of the dye molecules were taken up into the lysosomes, where it might be protonated owing to the highly acidified environment, resulting in the enhancement of fluorescent intensity. In more detail, we observed that the spherical structures stained by Lyso-BAM (green channel) were surrounded by LAMP1-mApple (red channel), the mApple labeled proteins on lysosome membrane, which coincided with our initial hypothesis. The crosstalk between the two channels were eliminated as shown in the bleed-through test in **Figure S3**. *Z*-stack colocalization of Lyso-BAM and LAMP1 further elucidated the above conclusion in a three-dimensional aspect (**Figure 6**). Additionally, the tile scanned imaging (**Figure S4**), which stitched multiple images into a larger mosaic, illustrated that this phenomenon was substantive universal rather than an individual exception. Compared to fluorescent proteins which different cells might have different expression efficiency, small molecule dye such as Lyso-BAM is able to stain all the cells homogeneously.

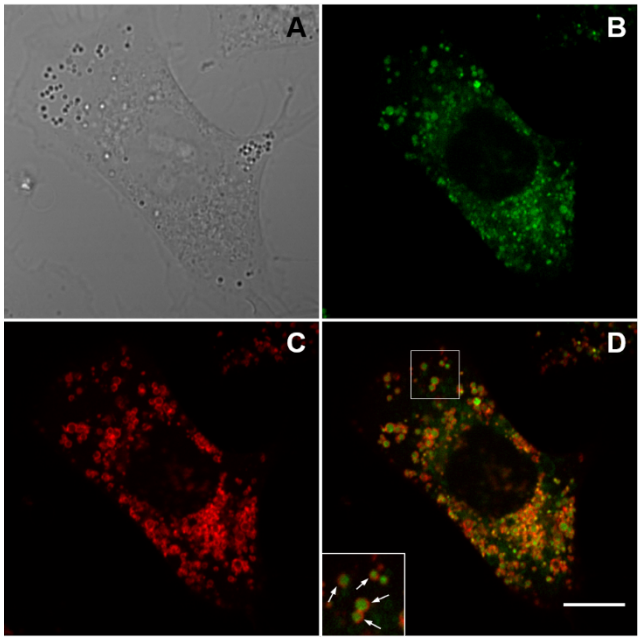

Figure 5. Confocal image of single LAMP1-mApple stable-expressed A549 cell stained with Lyso-BAM (25 μM) for 40 min. The bright-field image (A); the fluorescence image of Lyso-BAM channel under excitation of 488 nm laser (B, green) and LAMP1-mApple channel under excitation of 561 nm laser (C, red); merged image of the above fluorescent channels (D). Scale bar = 10 μm.

In summary, we have synthesized a series of AIE-active luminogens, BAMs, and further investigated its photophysical properties. By elaborately integrating the previously reported molecules, Me-BAM and Et-BAM, with newly designed molecules, Py-BAM, Morp-BAM and Lyso-BAM, into this work, we have a comprehensive comparison of the photophysical properties of the diaminomaleonitrile-functionalised Schiff base system. With different D-A moieties in their simple structures, these five molecules experienced different response to solvent polarity. Molecular modeling would be useful to further assist

the understanding of the structure-activity relationship. Aided by the alkylated morpholine functional group, Lyso-BAM showed better solubility compared with the other four compounds, making it applicable to visualize the intracellular lysosomes with high specificity. This work gives an augment of the family of diaminomaleonitrile-functionalized Schiff bases and multi-functional targeting would be developed by our group to provide more insight on lysosomal-related intracellular activities.

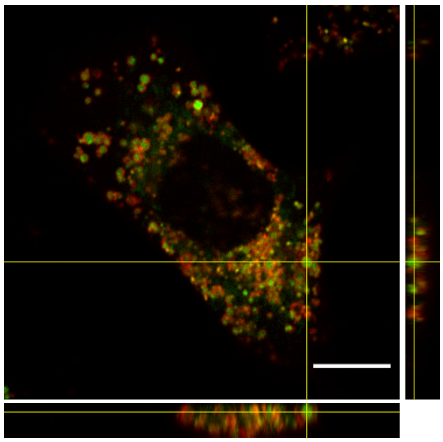

Figure 6. Orthogonal views of Lyso-BAM (green) and mApple (red) merged *z*-stack images. Scale bar = 10 μm.

Supplementary Materials

Dye synthesis, ^{1}H and ^{13}C NMR, HRMS spectrum, UV-vis spectra in different solvents, cell viability and cell images, are available on Journal's website.

CONFLICTS OF INTEREST

The authors declare no conflicts of interest.

ACKNOWLEDGMENT

We thank Dr Peter Lock and LIMS Bioimaging Platform, La Trobe University for the technical support and access to the confocal microscope. This work was supported by grants to Y.H. (Australian Research Council DE170100058 and Rebecca L. Cooper Medical Research Foundation PG2018043).

REFERENCES

1. Luo, J. D.; Xie, Z. L.; Lam, J. W. Y.; Cheng, L.; Chen, H. Y.; Qiu, C. F.; Kwok, H. S.; Zhan, X. W.; Liu, Y. Q.; Zhu, D. B.; Tang, B. Z., Aggregation-induced emission of 1-methyl-1,2,3,4,5-pentaphenylsilole. *Chem Commun* **2001,** (18), 1740-1741.
2. Parrott, E. P. J.; Tan, N. Y.; Hu, R. R.; Zeitler, J. A.; Tang, B. Z.; Pickwell-MacPherson, E., Direct evidence to support the restriction of intramolecular rotation hypothesis for the mechanism of aggregation-induced emission: temperature resolved terahertz spectra of tetraphenylethene. *Mater Horiz* **2014,** *1* (2), 251-258.
3. Qin, A. J.; Lam, J. W. Y.; Mahtab, F.; Jim, C. K. W.; Tang, L.; Sun, J. Z.; Sung, H. H. Y.; Williams, I. D.; Tang, B. Z., Pyrazine luminogens with "free" and "locked" phenyl rings: Understanding of restriction of intramolecular rotation as a cause for aggregation-induced emission. *Appl Phys Lett* **2009,** *94* (25).
4. Hong, Y. N.; Lam, J. W. Y.; Tang, B. Z., Aggregation-induced emission: phenomenon, mechanism and applications. *Chem Commun* **2009,** (29), 4332-4353.
5. Zhang, T.; Ma, H. L.; Niu, Y. L.; Li, W. Q.; Wang, D.; Peng, Q.; Shuai, Z. G.; Liang, W. Z., Spectroscopic Signature of the Aggregation-Induced Emission Phenomena Caused by Restricted Nonradiative Decay: A Theoretical Proposal. *J Phys Chem C* **2015,** *119* (9), 5040-5047.
6. Gu, Y. R.; Wang, K.; Dai, Y. X.; Xiao, G. J.; Ma, Y. G.; Qiao, Y. C.; Zou, B., Pressure-Induced Emission Enhancement of Carbazole: The Restriction of Intramolecular Vibration. *J Phys Chem Lett* **2017,** *8* (17), 4191-4196.
7. Leung, N. L. C.; Xie, N.; Yuan, W. Z.; Liu, Y.; Wu, Q. Y.; Peng, Q.; Miao, Q.; Lam, J. W. Y.; Tang, B. Z., Restriction of Intramolecular Motions: The General Mechanism behind Aggregation-Induced Emission. *Chem-Eur J* **2014,** *20* (47), 15349-15353.
8. Liang, G. D.; Lam, J. W. Y.; Qin, W.; Li, J.; Xie, N.; Tang, B. Z., Molecular luminogens based on restriction of intramolecular motions through host-guest inclusion for cell imaging. *Chem Commun* **2014,** *50* (14), 1725-1727.
9. Chen, J. W.; Law, C. C. W.; Lam, J. W. Y.; Dong, Y. P.; Lo, S. M. F.; Williams, I. D.; Zhu, D. B.; Tang, B. Z., Synthesis, light emission, nanoaggregation, and restricted intramolecular rotation of 1,1-substituted 2,3,4,5-tetraphenylsiloles. *Chem Mater* **2003,** *15* (7), 1535-1546.
10. Tong, H.; Dong, Y. Q.; Haussler, M.; Lam, J. W. Y.; Tang, B. Z., Aggregation-Induced Emissions of Pyran, Fulvene and Silole Derivatives. *Nonlinear Opt Quantu* **2006,** *35* (1-3), 147-154.
11. Zhao, Z. J.; Liu, D. D.; Lam, J. W. Y.; Lu, P.; Yang, B.; Ma, Y. G.; Tang, B. Z., Theoretical study of substituent effect on the charge mobility of 2,5-bis(trialkylsilylethynyl)-1,1,3,4-tetraphenylsiloles. *Sci China Chem* **2010,** *53* (11), 2311-2317.
12. Tong, H.; Hong, Y. N.; Dong, Y. Q.; Haeussler, M.; Li, Z.; Lam, J. W. Y.; Dong, Y. P.; Sung, H. H. Y.; Williams, I. D.; Tang, B. Z., Protein detection and quantitation by tetraphenylethene-based fluorescent probes with aggregation-induced emission characteristics. *J Phys Chem B* **2007,** *111* (40), 11817-11823.
13. Hong, Y. N.; Haussler, M.; Lam, J. W. Y.; Li, Z.; Sin, K. K.; Dong, Y. Q.; Tong, H.; Liu, J. Z.; Qin, A. J.; Renneberg, R.; Tang, B. Z., Label-free fluorescent probing of G-quadruplex formation and real-time monitoring of DNA folding by a quaternized tetraphenylethene salt with aggregation-induced emission characteristics. *Chem-Eur J* **2008,** *14* (21), 6428-6437.
14. Han, T.; Hong, Y.; Xie, N.; Chen, S.; Zhao, N.; Zhao, E.; Lam, J. W. Y.; Sung, H. H. Y.; Dong, Y.; Tong, B.; Tang, B. Z., Defect-sensitive crystals based on diaminomaleonitrile-functionalized Schiff base with aggregation-enhanced emission. *J Mater Chem C* **2013,** *1* (44).
15. Han, T.; Gu, X.; Lam, J. W. Y.; Leung, A. C. S.; Kwok, R. T. K.; Han, T.; Tong, B.; Shi, J.; Dong, Y.; Tang, B. Z., Diaminomaleonitrile-based Schiff bases: aggregation-enhanced emission, red fluorescence, mechanochromism and bioimaging applications. *J Mater Chem C* **2016,** *4* (44), 10430-10434.
16. Peng, L.; Xu, S.; Zheng, X.; Cheng, X.; Zhang, R.; Liu, J.; Liu, B.; Tong, A., Rational Design of a Red-Emissive Fluorophore with AIE and ESIPT Characteristics and Its Application in Light-Up Sensing of Esterase. *Anal Chem* **2017,** *89* (5), 3162-3168.
17. Lawrence, R. E.; Zoncu, R., The lysosome as a cellular centre for signalling, metabolism and quality control. *Nat Cell Biol* **2019,** *21* (2), 133-142.
18. Kawai, A.; Uchiyama, H.; Takano, S.; Nakamura, N.; Ohkuma, S., Autophagosome-lysosome fusion depends on th pH in acidic compartments in CHO cells. *Autophagy* **2007,** *3* (2), 154-157.

19. Leung, C. W.; Wang, Z.; Zhao, E.; Hong, Y.; Chen, S.; Kwok, R. T.; Leung, A. C.; Wen, R.; Li, B.; Lam, J. W.; Tang, B. Z., A Lysosome-Targeting AIEgen for Autophagy Visualization. *Adv Healthc Mater* **2016,** *5* (4), 427-31.
20. Lippert, E., Losungsmittelkorrektur Und Unechte Maxima in Absorptionsspektren. *Angew Chem Int Edit* **1955,** *67* (22), 704-704.
21. Mataga, N.; Kaifu, Y.; Koizumi, M., Solvent Effects Upon Fluorescence Spectra and the Dipolemoments of Excited Molecules. *B Chem Soc Jpn* **1956,** *29* (4), 465-470.
22. Fan, F. K.; Nie, S.; Yang, D. M.; Luo, M. J.; Shi, H.; Zhang, Y. H., Labeling Lysosomes and Tracking Lysosome-Dependent Apoptosis with a Cell-Permeable Activity-Based Probe. *Bioconjugate Chem* **2012,** *23* (6), 1309-1317.
23. Cohen-Dvashi, H.; Israeli, H.; Shani, O.; Katz, A.; Diskin, R., Role of LAMP1 Binding and pH Sensing by the Spike Complex of Lassa Virus. *J Virol* **2016,** *90* (22), 10329-10338.